ACS OMEGA

http://pubs.acs.org/journal/acsodf

Article

# Consumer-Grade Inkjet Printer for Versatile and Precise Chemical Deposition

Nikolaj Kofoed Mandsberg,* Jesper Højgaard, Shreya Suhas Joshi, Line Hagner Nielsen, Anja Boisen, and En Te Hwu

Cite This: *ACS Omega* 2021, 6, 7786−7794

Read Online

ACCESS | Metrics & More | Article Recommendations | Supporting Information

**ABSTRACT:** Two simple, mechanical modifications are introduced to a consumer-grade inkjet printer to greatly increase its applicability. First, roller isolation bars are added to unlock multiple prints on the same substrate without smearing. This enables printing on a diverse set of substrates (rigid, elastic, liquid, granular, and sticky). Second, spring loadings are added to increase the print precision up to 50-fold, which facilitates alignment to a pre-patterned substrate or between successive prints. Utilizing the expanded substrate compatibility and the increased print precision, we explore tunable loading of drug combinations into microdevices. This loading method has promising applications within point-of-care personalized medication. Furthermore, we show how inkjet printers with array-type printheads (in our case, 6 x 90 nozzles) allow for quasi-simultaneous loading of reactants into microfluidic systems. The ability to do a quasi-simultaneous introduction of chemicals may be particularly useful for studies of rapidly reacting systems of three or more reactants, where premature introduction can shift the initial conditions from the intended. We believe that our modifications to an affordable system will inspire researchers to explore the possibilities of inkjet printing even further.

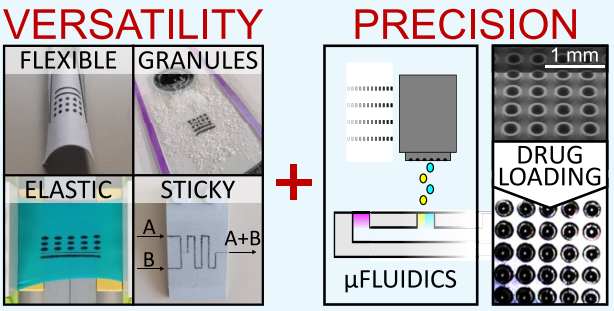


## INTRODUCTION

Photonic crystals,[1−4] tissue engineering,[5] (bio)chemical sensing devices,[6] drug loading[7−11] and discovery,[12] droplet microarrays[13] including emulsion droplets[14] for polymerase chain reaction,[15] fabrication of microfluidics,[16−18] metamaterials,[19] and flexible electronics[20]—these are just a few examples of applications of high-end inkjet printing. The on-demand droplet production and diverse material compatibility make it possible for inkjet printing to offer both easy customization and short iteration times. Compared to many traditional fabrication methods, this flexibility allows the individual printer to serve multiple purposes, which is much preferred from both a consumer and an environmental perspective. Clearly, access to inkjet systems could be beneficial for many researchers and across most research fields.

Despite the advantage of owning a high-end inkjet system, its typical price tag of $10,000 likely makes most research labs hesitate with an acquisition. Probably for that same reason, many studies present adaptation of consumer-grade inkjet printers that typically cost a tenth or less. These inexpensive inkjet printers show compatibility with widely different ink choices and the ability to print electrical circuits,[21] crystal seeds,[22] sensors,[23,24] wettability patterned substrates,[25,26] microfluidics,[27,28] and more.[29−35] They can even offer control over the individual inkjet nozzle in an array-type printhead.[36]

While these consumer-grade inkjet systems already have found widespread applications, they all share at least two limiting characteristics. First, they all print on unprotruded substrates, and second, they all only do first-prints. Most often, consumer-grade printers have friction-based rollers for substrate feeding, but exactly that causes both incompatibility with most protruded substrates and smears out already deposited ink when printing multiple times. Furthermore, some almost unnoticeable uncertainty in the print position always exists due to backlash. For first-prints, this small imprecision often does not matter, but for multi-step fabrication processes, half a millimeter in misalignment can be detrimental. We conclude that there is a need for an inexpensive solution, which overcomes these limitations on substrate choice and with poor repeatability so researchers can test the ideas that require more exotic substrates and/or reliable alignment.

Therefore, we present modifications to an inexpensive (~$300) consumer-grade inkjet printer (Epson EcoTank

**Received:** January 16, 2021
**Accepted:** February 19, 2021
**Published:** March 9, 2021

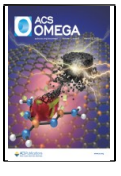

L805) to overcome these two limitations. Furthermore, we discuss how this inkjet solution can outperform high-end systems on certain characteristics. This is possible by paying special attention to the strengths of our consumer-grade photo printer, which benefits from decades of optimization in speed, DPI (dots per inch), and miniaturization. After initially describing the modifications, we systematically study the improved repeatability, the ability to print quasi-gradients (which arises from the high speed and DPI), and the broadened substrate compatibility spanning protruded substrates and more atypical ones. Finally, we do two small demonstrations that in different ways take advantage of our system's strengths. The first pertains to the loading of drugs in microcontainers (microdevices intended for oral drug delivery) and the second to the loading of reactants in microfluidic systems.

## RESULTS

**Printer Modification and Characterization.** In this section, we describe the printer modifications that lead to the high repeatability and enable alignment to a pre-patterned substrate or between successive prints. Next, we quantify this improved performance and print on various substrates to exemplify the broadened substrate compatibility.

*Modifications to the Printer.* Two simple (Figure 1) and quickly implemented mechanical modifications are made to overcome the typical issues with smearing and misalignment (convenience modifications were also introduced as seen in Figure S1, but these do not affect the two main issues). First, adding roller isolation bars creates a distance from the substrate to the feeding rollers, which obsoletes the requirement of an unprotruded substrate and stops smearing (Figure 1a,b). With our choice of isolation bars (either electrical wires or a cut DVD attached with double-sided tape), about 10% of the print area is sacrificed to significantly increase the versatility of the remaining 90% (see Figure S2 for a print homogeneity test over the printing area). Second, two spring loadings are introduced, one pulling the DVD tray feeder toward the left side and one pushing the DVD tray to the left inside the feeder (Figure 1c). The spring loads reduce the misalignment in the repeated print from >500 $\mu$m to a sub-visual level (we quantify the improvement in the next section). Together, the isolation bars and the spring loads enable repeated prints and significantly improve the precision in the print position.

*Improved Performance and Versatility of the Printer.* Before turning to the demonstrations, we characterize relevant print characteristics and briefly show the increase in versatility: we characterize the precision/misalignment in repeated prints more extensively, we investigate the ability to print gradients, and we show prints on substrates of various natures. For the subsequent demonstrations, the reader will find that they have been enabled by different combinations of the improved aspects.

We used a test pattern comprising four 450 $\mu$m squares for characterizing the precision upon repetitive printing. We printed each test pattern (1, 2, 3...) with an offset of 1800 $\mu$m from the previous to easily distinguish the individual prints (Figure 2a, right, N.B., some squares have an ink line detached, which is due to the print driver's conversion from a continuous shape into one compatible with the discrete nature of the nozzle array). The positions of the individual prints were determined via a MATLAB script. In brief, the image

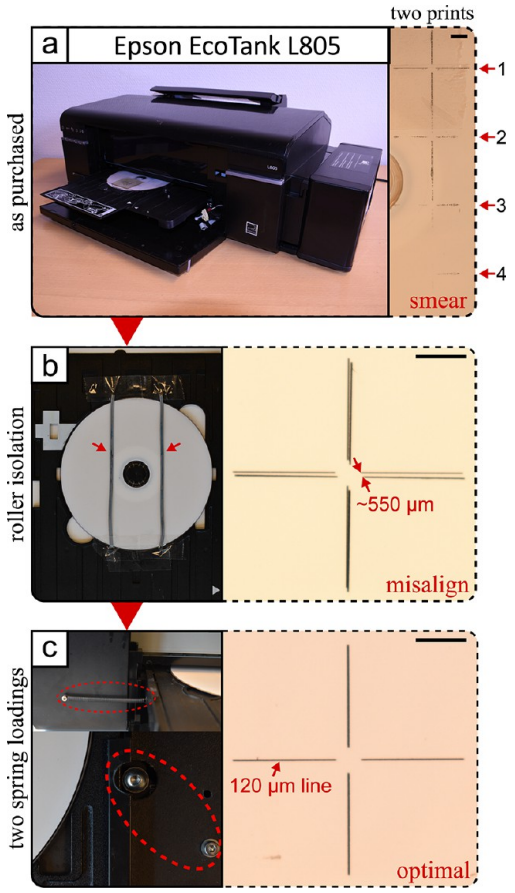


**Figure 1.** Two simple mechanical printer modifications (to the left) and their effects on printing an aiming cross twice (to the right). (a) As-purchased printer smears out the first cross and misaligns the second. (b) Adding roller isolation bars removes the smearing, but the misalignment (550 $\mu$m) persists. (c) Introducing two spring loadings (encircled with red) significantly reduces the uncertainty in the tray position, which improves alignment to a sub-visual level as is evident from the two crosses printed on top of each other. The scale bars are 5 mm.

underwent a binary conversion using Otsu's method for threshold, the connected components were determined using the built-in function bwconncomp ($n$ = 8), and the positions of the contained pixels were weighted using their respective grayscale value to find the center of each print. Subtracting positions of successive prints and the offset gave the marginal misalignment (see Materials & Methods and Figure S3 for a more detailed description of the analysis). The misalignments (in both $x$ and $y$ direction) as a function of print number (1, 2, 3...) are plotted in Figure 2a (left) and are generally randomly distributed around zero, indicating no continuous drift, which indicates a good stability of the system without the need for regular readjustments. The first four prints are all negative, which can be by coincidence or due to a slight initial relaxation of the mechanical system (i.e., DVD tray and feeder position). Overall, a reduction in misalignment from ~550 $\mu$m to approximately 10 $\mu$m is evident, which allows for applications where such high precision is required.

As a next thing, we characterized the ability to print gradients, something that is particularly interesting as it benefits from the decade-long industrial optimization of speed and droplet density. Applications of these gradients include screening where all concentrations in a given range are


https://dx.doi.org/10.1021/acsomega.1c00282
ACS Omega 2021, 6, 7786−7794

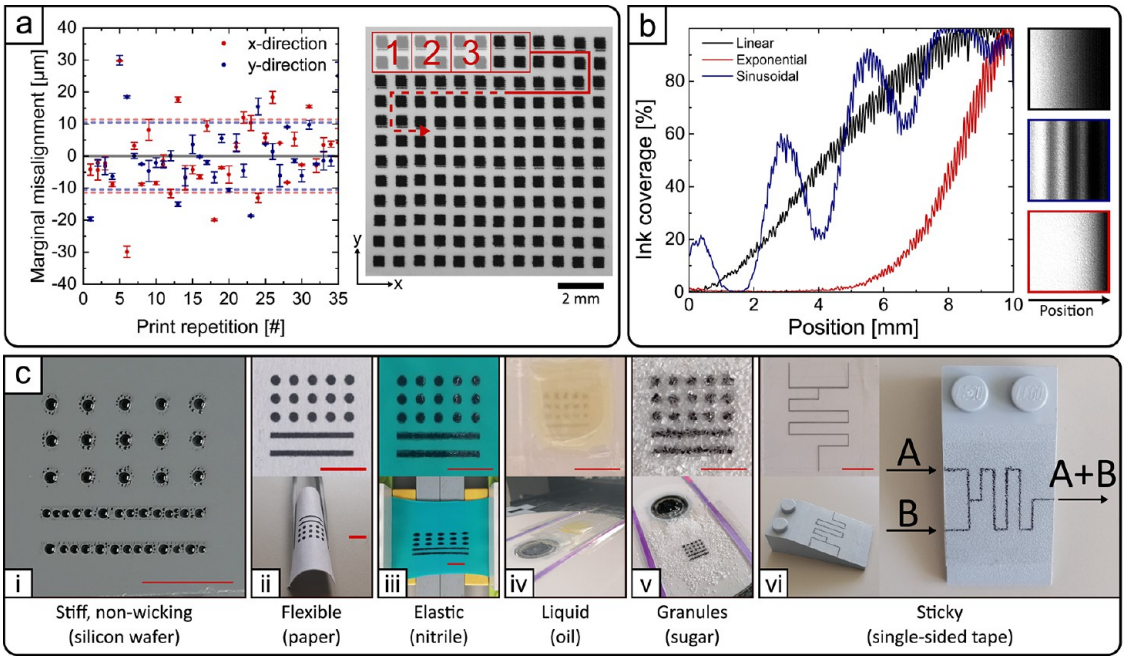


**Figure 2.** Characterization and exemplification of improved performance. (a) Test of the precision in print repeatability, where the marginal misalignment is calculated as the discrepancy between the measured and designed print position (the dashed lines are the calculated standard deviations). On the right is the optical microscopy image of the printed pattern with the two-by-two unit cell together with its stepping procedure. The squares and spaces are both 450 $\mu$m. (b) High DPI of the photo printer (up to 5760 × 1440) unlocks the printing of pseudo-gradients. Here, we print three common 1D gradients and characterize them by measuring the average pixel intensity in the vertical direction. To the right, the optical microscopy images of the three gradients are shown. (c) Introduction of roller isolation bars also allows printing on a diverse set of substrates. We present a subset hereof, including (i) stiff and non-wicking, (ii) flexible and wicking, (iii) elastic, (iv) liquid, (v) soluble granules, and (vi) sticky.

investigated. In our characterization, we printed three common gradients, namely, a linear, an exponential, and a sinusoidal. The results are seen in Figure 2b. The gradients are not perfectly smooth but exhibit some oscillations due to the finite number of nozzles (nozzle−nozzle distance of 60 $\mu$m). The period of observed oscillations is ∼100 $\mu$m. At first, it may seem like an issue, but it is only so when the relevant length scale of the intended application is compared to the period of these oscillations. In addition, with some ingenuity, it could probably be used for one's advantage, perhaps as local concentration minima acting as, e.g., cell traps?

We exemplify the expanded range of possible substrates, which no longer is restricted to those that are both stiff and unprotruded (Figure 2c). We present a diverse set of substrates (including flexible/stiff, wicking/non-wicking, solid/liquid, granular, and sticky) with their individual advantages. The non-wicking allows to make pico- to nanoliter-volume digital droplet reactors (Figure 2c-i);[37−39] the paper can be used for paper-based microfluidics via its wicking (Figure 2c-ii);[40−42] flexible substrates offer the possibility to increase the resolution in one direction by sacrificing resolution in the orthogonal direction (Figure 2c-iii).[43,44] In addition to solid continuous materials, we also print on both liquid substrates (oil, Figure 2c-iv) and granular (sugar, Figure 2c-v), which would otherwise have been displaced by the rollers in the absence of our roller isolation bars. We imagine that printing atop of a granular/colloidal material could be used to create macro-scale patterns of self-assembled colloids, e.g., print sol−gel to induce evaporative, colloidal co-assembly.[45]

As a last type of substrate, we show printing on sticky materials (e.g., single-sided tape, Figure 2c-vi). One of the applications we envision is within the rapid prototyping of microfluidics; hence, we named the approach "sticky fluidics". A desired fluidic layout is printed on tape, which subsequently is attached to a non-wicking surface; here, a LEGO brick. Besides resembling the rapid prototyping of surface microfluidics, it has advantages over this such as an increased pressure barrier (similar to the advantage of freestyle fluidics[46] but with the potential of an even larger pressure barrier due to the solid barrier, i.e., tape). Contrary to many other microfluidic systems, the sticky fluidics is not restricted to planar designs but can be bent around corners, which allows novel circuit layouts. In summary, this sticky fluidics can offer rapid microfluidic prototypes with large pressure breakdown values that are not restricted to planar layouts.

**Demonstrations.** With the hope to inspire fellow researchers to explore new applications of consumer-grade inkjet systems, we now present two different demonstrations. The first relates to personalized medicine via tailorable, waste-free drug loading of microcontainers and the second to microfluidics, where we, in a quasi-simultaneous way, inject reagent combinations into individual inlets. The demonstrations purposely take advantage of the introduced roller spacing, the alignment possibility, and the commercial photo printer's speed and DPI.

*Drug Loading: Personalized Medicine via Inkjet Printing.* Oral delivery is often the preferred route of drug administration due to its convenience for patients. However, physical barriers in the body, the low pH of the stomach, and enzymatic degradation in the gastrointestinal tract can limit bioavailability upon oral administration.[47,48] Therefore, microcontainers, one type of microdevices (SEM micrograph in Figure 3a-left), have


https://dx.doi.org/10.1021/acsomega.1c00282
ACS Omega 2021, 6, 7786−7794

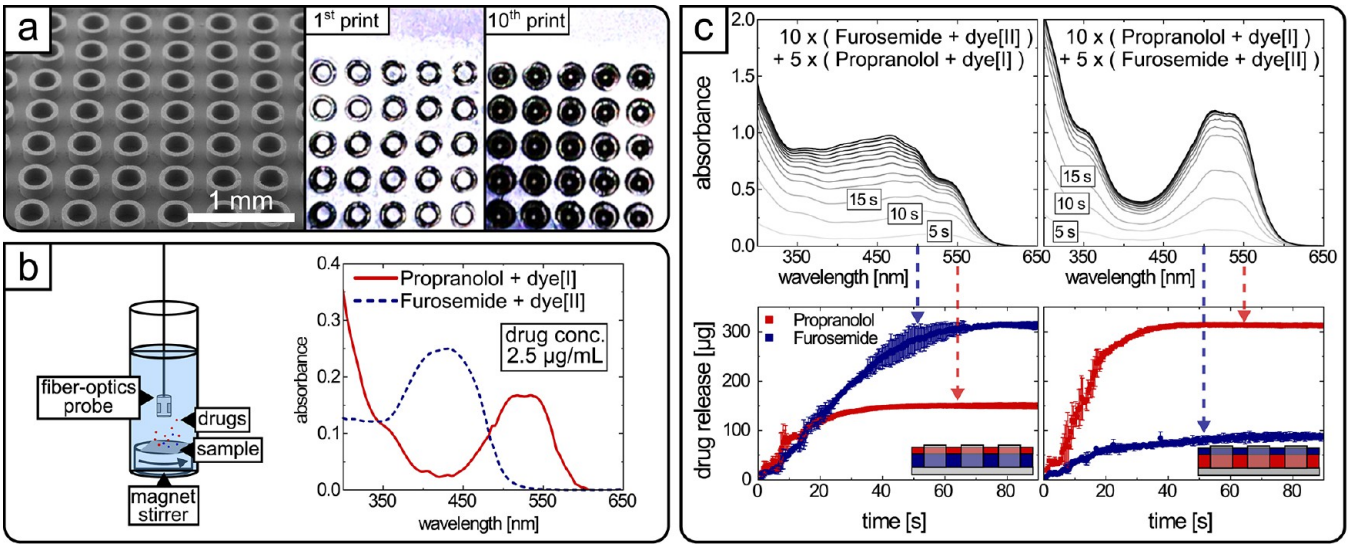


**Figure 3.** Inkjet loading of drugs into microcontainers for personalized medicine. (a-left) Tilted SEM micrograph showing the microcontainers prior to drug loading. (a-right) Optical microscopy images of the microcontainers after the 1st and 10th print, which demonstrates the possibility to do tailored loading with minimal waste. (b-left) Illustration of the UV−VIS *in situ* microdissolution system for measuring the amount of drug released into the solution at a given time. (b-right) Unmixed absorption signals for the two drugs/dyes mixtures. (c-top) Temporal drug release spectra from microcontainers loaded with first 10 doses/layers of either propranolol or furosemide and then 5 doses/layers of the other drug. (c-bottom) Using the unmixed signals, the temporal spectra are decomposed to visualize the release kinetics for the individual drugs in the two loading examples.

developed as a concept, offering protection of the drug until it arrives at the intestinal wall where the drug can be released from the microcontainers and then enter the bloodstream.[47,49−51] Before administration, the drug must be loaded into the microcontainers, which can be a challenge due to their small size.

With our improved repeatability, it is possible to load the microcontainers with a consumer inkjet printer. Before modification, this was not possible due to a marginal misalignment comparable to the lateral container dimension (~230 $\mu$m, recall Figure 1b and Figure 3a-left). By first printing an alignment pattern on a DVD and subsequently aligning the microcontainer chip hereto using a micromanipulator, we load the microcontainers with a solution and with minimal waste (see Figure S4). Multiple printing runs fill up the microcontainers as seen in Figure 3a-right. With this inkjet system, microcontainers can be loaded with a single drug or a combination of up to six drugs (by the use of the six ink channels of the printer).

In this demonstration, we chose just two model drugs, furosemide and propranolol, to simplify the decomposition of the signals in a subsequent *in vitro* release study. The drugs are printed in mixtures with printer inks/dyes (yellow and magenta, respectively) to easily confirm their printing via visual inspection (the mixing with ink is not critical, but it is convenient at a technology-development-stage). The release study was performed with a UV−vis spectrometer *in situ* microdissolution setup (MicroDISS Profiler, Pion Inc., USA) depicted in Figure 3b-left and the decomposition via the construction of calibration curves in advance (Figure 3b-right shows examples of the unmixed signals used for the calibration). To enhance the signal in the release study, we loaded the drug mixtures both in and between the microcontainers. This was done to better resolve and demonstrate the tunable release kinetics, but the solutions (although smaller amounts) can be printed only into the microcontainers as evident from Figure 3a-right. After printing of 15 drug layers (10 of one drug and 5 of the other; each layer is estimated to contain 40 nL of drug solution by assuming a droplet−droplet pitch equal to the nozzle−nozzle pitch and a single droplet volume of 1.5 pL), the solvents were evaporated, and the release kinetics (under stirring) were characterized. The temporal spectra are seen in Figure 3c-top, and the release curves for the individual drugs are presented in Figure 3c-bottom (the signals were decomposed using the absorptions at 552 and 500 nm). We see how the total dose is adjusted via the number of layers but also how the release rate (the slope of the release curve) can be tuned by changing the order of the API layers. The stability of the APIs during the inkjet printing depends on the drug, but for a piezo printhead, only shear stresses may influence the structural stability.[52,53]

Previously, research groups already explored inkjet printing to load planar microdevices,[7,9−11] even to create the microdevices themselves by printing 5% polymeric solution (Eudragit FS 30 D), which upon evaporation forms the microdevice via the coffee ring effect.[8] These existing examples all use high-end systems, which are unaffordable for most research groups where the development of the inkjet platform is not the focus. Our inexpensive alternative allows most research groups to explore this direction without a large investment. Furthermore, while these high-end systems are typically optimized for precision and volumetric throughput, they are at points less flexible than a photo printer is. A photo printer allows for the simultaneous loading of tailored drug combinations and thereby tunable drug release profiles. While we loaded the different drugs in separate layers, they can alternatively be loaded side by side or as a combination of both, resulting in different compositions of neighboring microcontainers' load. The ability to tailor the drug combination on a case-by-case basis can be combined with the printing of polymer lids of different selective adhesion or degradation properties (e.g., pH dependency,[54] enzyme


https://dx.doi.org/10.1021/acsomega.1c00282
ACS Omega 2021, 6, 7786−7794

sensitive,[55] and degradation rate[56]). In that way, different dose levels can be delivered to different parts of the gastrointestinal tract.

*Microfluidics: Quasi-Simultaneous Loading of Reactants.* The second demonstration elucidates new possibilities within the reactant loading of microfluidics. Here, the consumer-grade inkjet printer offers several advantages over pipette loading or even loading via a high-end inkjet system. The pipetting system (even pressure wave assisted[57]) does not produce equally small droplets, which is problematic as it limits the downscaling of the microfluidic system. The high-end inkjet systems can deliver picoliter droplets but often have far fewer nozzles (often just one) than the consumer-grade array-type printhead (here with 6 × 90 nozzles). One great advantage of an array-type printhead is the possibility to do quasi-simultaneous loading, i.e., to load multiple reactants (typically up to four or six) in the same or different inlets within milliseconds.

Figure 4a shows a schematic of the quasi-simultaneous loading of a microfluidic system. For this demonstration, a

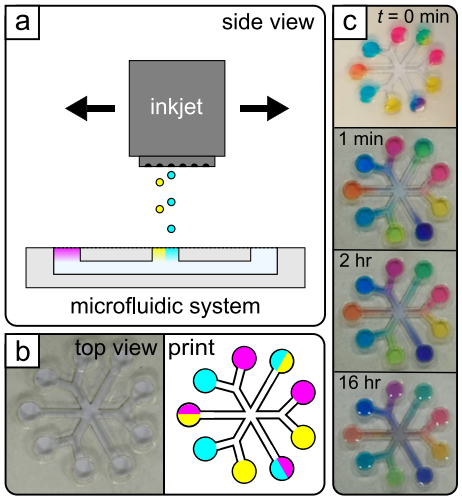


**Figure 4.** Quasi-simultaneous injection of multiple reactants into a microfluidic system. (a) Schematic of the inkjet system during the reactant loading of the microfluidic system. (b-left) Top view of fabricated microfluidic demo together with the (b-right) test pattern for the demonstration. (c) Time-series photographs of diffusive mixing in the microfluidic system.

microfluidic system with nine inlets (diameter of 2.5 mm) was prepared via layer-by-layer assembly of 100 $\mu$m-thick $CO_2$ laser cut polymethyl methacrylate sheets (see Figure S5 for further details on the fluidic layout and experimental setup). A top-view image of the fluidic system is shown in Figure 4b-left and the loading pattern in Figure 4b-right. This pattern is designed with identical loading volumes (estimated to be 2 nL) of all inlets, but three of the inlets have quasi-simultaneous loading of two reactants. Figure 4c shows the temporal evolution of this diffusive system with photographs taken after 0 min, 1 min, 2 h, and 16 h The photo from immediately after loading ($t$ = 0 min) shows how the loading of multiple reactants in the same inlet well is possible with little droplet impact-induced mixing.

Several other advantages in reactant loading arise from using an inkjet system and particularly an array-type one. While the introduction of two reactants to each other is also possible using a pipette, the simultaneous introduction of three or more becomes severely challenging. If the critical reaction time scale compares to or is shorter than the pipetting time, then the system will already have changed when the third reactant is introduced. Furthermore, the inkjet system allows for a repeated or semi-continuous introduction of more reactants with only little impact-induced mixing due to the small droplet size. Also, it empowers sub-picoliter adjustment of the ejected droplet's volume, facilitating delicate tuning of the loaded reactant volume. This ability to load reactants as thousands of small (picoliter) volumes, as compared to a few larger volumes, allows for a smoother increase in the system's reactant concentration. This is, for example, highly relevant in the cryopreservation of oocytes as the addition of cryoprotectants (CPAs) can be toxic if the change in concentration is too abrupt, so protocols have been developed with step-wise addition of CPAs to the cells.[58] Here, the inkjet system with its delivery of digit picoliter volumes can be a much-needed tool for providing the smooth concentration gradient needed to minimize toxicity. Finally, the array-type inkjet system allows for more complicated initial conditions in reactant distribution, which can perhaps be utilized in block copolymer self-assembly systems to have lateral functionality gradients emerge.

## DISCUSSION

In the following, we further discuss strengths, weaknesses, and opportunities of this consumer-grade inkjet system. First, in this study, we demonstrated the improved performance mostly using the supplied printer inks, but the choice of a piezo-type printer means compatibility with both non-volatile and heat-sensitive "inks". To this end, other studies have demonstrated consumer-grade inkjet printing of liquids containing mammalian cells,[59] bacteria,[60] polymers,[61] conductive materials,[62] and colloids[63] just to mention a few. That said, further optimization of the compatibility is still needed as evidenced by frequently reported issues with nozzle clogging.

For drug loading, nozzles prone to clogging may require using lower drug concentration and that reduces loading efficiency. A recent study by Modak et al. showing improved mass loading may alleviate this issue.[64] Still, many solid drugs are poorly water-soluble resulting in a small loading efficiency, e.g., furosemide has a solubility of ∼1 wt/vol % (typical commercial solution with pH 8.0−9.3), leading to unreasonable long loading times for human dosage levels. The loading efficiency could also be improved via surface functionalization of the microcontainers,[7] but further hardware and software modifications are likely needed before the system performs sufficiently well. In particular, rewriting the printer driver to allow control over the individual nozzles (similar to what Waasdorp et al. did[36]) will reduce time spent on unnecessary head movement. Also, incorporation of a heating element would allow for continuous operation loading rather than a batch-like process, where the containers are alternately being filled and heated for solvent evaporation. This thermal treatment could of course mean a decreased compatibility with temperature-sensitive drugs. Incorporation of camera-assisted alignment of the print to the chip (rather than the opposite) will also greatly improve the usability. If these upgrades are made and the drug loading system is FDA approved, then it may one day be possible for consumers to daily have the optimal drug combinations printed out at home in a point-of-care (PoC) fashion.

We also investigated the ability to print gradients, which has applications such as functionality gradient for sensing[65] or liquid guiding.[66] Another impactful use of printed gradients lies within the interaction between bacteria and antibiotics. Here, a


https://dx.doi.org/10.1021/acsomega.1c00282
ACS Omega 2021, 6, 7786−7794

standard experiment is the determination of the minimum inhibition concentration (MIC)[67] done in either liquid media or on plates of a solid growth medium. Using inkjet gradient printing, we envision that this experiment can be sped up significantly via more pronounced parallelization. The advantage over other MIC methods becomes even larger when printing orthogonal gradients of two antibiotics to determine the combined MIC. This is relevant since combinations of antibiotics are often administered and collecting data hereon is time and resource consuming due to the non-linear scaling (here, $N^2$) of combinatorial chemistry. To realize the inkjet MIC, agar plates with bacteria can be prepared to fit the DVD tray and hereon, antibiotics (e.g., ciprofloxacin) are printed as either discrete regions or a semi-continuous gradient (see Figure S6). For a 2D system, the Brownian mean square displacement is $x = \sqrt{4Dt}$, where $D$ is the diffusion constant and $t$ is the time. The characteristic time for diffusing an oscillation period of 100 $\mu$m (revisit Figure 2b) is for ciprofloxacin in water (with $D = 4\times10^{-10}$ m$^2$/s) about 6 s. Thus, antibiotic diffusion expectedly will smooth out the oscillations. With this faster method for MIC determination, personalized antibiotic dosing will also be made easier. In the Supporting Information, we present some development in this direction as a guide for future studies.

Lastly, we discuss a few applications where inkjet printing may bring novelty. First, within the marriage between bottom-up and top-down fabrication, patterned self-assembly or assembly gradients could be made easier with inkjet printing. A printed liquid pattern can exert a rationally designed capillary force to locally tune the morphology of an otherwise homogeneous system. This is beneficial since industrial productions can then be optimized for producing a single material that is subsequently tuned for the specific application. A second application is within anti-counterfeit, where unique molecular fingerprints on surface-enhanced Raman spectroscopy (SERS) substrates can be printed on high-end products or cases where the absence of tampering is paramount (e.g. drugs for medical treatment). A third application is the printing of crystal seeds for spatially controlled crystal growth.[22] Previously, crystal growth has been directed via self-assembled monolayers,[68] but inkjet printing offers on-demand flexibility. One use is within drug monitoring, where a recent study characterized bulk drug properties by measuring the resonance properties of single drug particles.[69] Printing a seed pattern of this drug could enable the parallelization of this characterization method to speed up data collection. The fourth, and last, suggested application is camera-assisted spatially adaptive dosing, where events in a 2D system could be monitored with a camera and inkjet interventions could be made as per desire. For instance, this could either be as negative and/or positive feedback mechanisms or could be as an alternative to optical tweezers for cell movement in photosensitive cases. Here, the movement of cells could be guided via the injection of nutrients in a 2D reservoir containing the cells.

## CONCLUSIONS

We introduced simple, mechanical modifications to a consumer-grade printer to overcome typical issues with smearing and poor repeatability. The improved repeatability unlocks alignment to a pre-patterned substrate or between successive prints with a marginal misalignment of about 10 $\mu$m. The introduction of roller isolation bars solves the issue with smearing and also enables printing on diverse substrates, such as protruded, liquid, granular, and sticky, all with each of their set of advantages. The original purpose of photo printing provides a DPI sufficiently high to print gradients that are particularly useful for screening/sensing applications. Our improvements, together with the long-lasting optimization of consumer-grade printers, unlock a vast number of applications, two of which we briefly touch upon. We demonstrate (1) how the improved alignment means that liquid drugs can be efficiently loaded into submillimeter containers, which is a possible pathway for PoC personalized medicine, particularly when it becomes possible to screen people's health and optimize their medication plan daily. Second is (2) that the inkjet injection of reactants into a microfluidic system can be done quasi-simultaneously due to the array-type printhead and high speed of the consumer-grade inkjet system. Lastly, we briefly discuss the advantages of low-cost inkjet printers for the field of combinatorial chemistry. We believe to have proven the usefulness of such a system and inspired researchers to further explore new applications.

## EXPERIMENTAL SECTION

**Inkjet Printer, Image Analysis, Reagents, and Materials.** We used a piezoelectric inkjet printer of type Epson EcoTank L805, but the modifications can be applied to other types (such as thermal types) or brands of inkjet printers with an optical disc (CD/DVD/Blu-ray) printing function. More precisely, the roller isolation bars work with printers having a friction-based feeding mechanism and the spring loading when there is a large clearance to close. Both are common for consumer printers. For the characterization, we analyzed all images with scripts written in MATLAB R2017b. Reagents used were DL-propranolol (Acros Organics, Geel, Belgium), furosemide (Fagron, Uitgeest, The Netherlands), and ciprofloxacin hydrochloride (Fagron, Uitgeest, The Netherlands). The microcontainers were loaded with furosemide and propranolol mixed with yellow and magenta Epson printer ink/dye, respectively. The drugs had inks added to allow easy, visual confirmation of their printing.

**Demonstrations.** In brief, the methodology regarding the demonstrations is as follows (more details provided in the following sections and the Supporting Information). Microcontainers were fabricated by photolithography in SU8, while the microfluidic system was a layer-by-layer assembly of 100 $\mu$m-thick polymethyl methacrylate sheets using double-sided tape.

**Two Small Printer Modifications.** Overcoming the two severely limiting issues, namely, smearing and misalignment, required two small modifications. First, the rollers feeding the substrate into the printer cause the smearing as they are in contact with the area being printed on. However, the rollers are mounted with springs, which makes it possible to install roller isolation bars on the substrate. They lift the rollers from the substrate to enable multiple prints without smearing. Our choice of bars does decrease the printable area by 5−10%, but this number is easily reducible. Second, a gap of about 500 $\mu$m exists to ease the DVD tray insertion. Consequently, a comparable uncertainty is risked in the tray position from one tray loading to the next, which makes deliberate alignment difficult. Therefore, two spring loadings are added to minimize this backlash-induced position uncertainty.

**Printer Characterization.** The repeatability in the print position is critical to alignment. To assess this performance


https://dx.doi.org/10.1021/acsomega.1c00282
ACS Omega 2021, 6, 7786−7794

characteristic, a print pattern comprising two-by-two squares of size 450 with spacing 450 was stepped 36 times using a pitch of 1800 $\mu$m. The choice of 450 $\mu$m matches the pitch of the microcontainer array but could be decreased. The minimum feature size is governed by the substrate, and the single droplet volume (approximately 1.5 pL), which in our case resulted in a 40−70 $\mu$m diameter spot. The ability to print squares is limited by this spot size. Furthermore, we experimentally determined the minimum spacing between features to be between 90 and 160 $\mu$m. To assess the alignment, optical microscopy images (Zeiss Axio Zoom.V16, Zeiss, Germany) of the 450 $\mu$m pitch test print were captured. The marginal misalignment was assessed with a tailored MATLAB R2017b script. The script initially rotates the image so that it aligns with the print direction. Subsequently, a mask is created from the image using the im2bw function with Otsu's method and eroded so that only background pixels are preserved. Using this mask, the average background intensity level is calculated and subtracted from the original image and simultaneously inverted. In this image, the connected components are identified using the bwconncomp function and subsequently labeled. Each component then has its center of mass calculated using the inverted, background-corrected image as eight. Now, using the centers' $x$ and $y$ coordinates, the prints are grouped according to the print design (two by two groups), and the average position is found as a simple mean. Finally, it calculates the marginal misalignment as the difference between the expected print center location and the measured one.

The ability to print gradients (and not just black/white) allows spatial heterogeneity (other than binary) in reactant amounts with a single print. Therefore, we choose to characterize also this important aspect of the printer. Three 1 megapixel square images with distinct gradients (linear, exponential, and sinusoidal) were generated in MATLAB R2017b and printed on DVD substrates. Optical images (pixel size = 6.5 $\mu$m) of the 10 by 10 mm prints were captured with a Zeiss Axio Zoom.V16. Each image was corrected for both background and the non-zero pixel value of the black ink to obtain the presented graphs.

**Drug Loading Demonstration.** With the inkjet printer, the drug in solution was loaded onto a 13 by 13 mm silicon chip containing a 625 cylindrical microcontainer (~230 $\mu$m inner diameter and ~250 $\mu$m height with fabrication already described in the literature[70]). Two model drugs, furosemide and propranolol, were chosen for the loading demonstration and subsequent drug release characterization. In this demonstration, we chose to mix the drugs with Epson printer ink to make the printing more apparent (1 mg/mL furosemide and 10 mg/mL propranolol aqueous solutions were mixed 50/50 with yellow and magenta ink, respectively). Following 15 print repetitions, the solvents (non-proprietary: water and glycerol)[71] were evaporated by placing the chips on a hotplate for 30 min at 190 °C. Using double-sided carbon tape, the chips were mounted on cylindrical stirring magnets (100 rpm) and loaded into 30 mL cylindrical glass vials. Then, 10 mL Milli-Q (18.2 MΩ) was added to each vial to initiate the drug release and spectra (200−720 nm) were collected with a frequency of 10.87 Hz. In addition, reference spectra were collected for all both drug−dye combinations to construct the calibration curves for the wavelengths 500 and 552 nm used in the signal decomposition. Error bars are standard deviation ($n$ =2).

**Microfluidic Demonstration.** The microfluidic system comprises a bottom, mid, and top layer in polymethyl methacrylate (PMMA) (laser cut on a CO2 laser: 30 W, 24 × 12; Epilog Laser Mini, CO, USA). The 100 $\mu$m-thick layers were assembled using double-sided tape, and the microfluidic system was prefilled with DI water using a 200 $\mu$L pipette. The DI water was pipetted into the channel at one inlet, and it was done slowly to not exceed the pressure barrier in the other inlet/outlet channels, which would otherwise complicate the prefilling of the microfluidic system. The chip was mounted in a customized holder and loaded into the printer. Epson inks were used for this demonstration, and the chosen test pattern was printed one time to load the microfluidic system. A time-lapse video was captured using a Nikon D5600 in automatic mode. Frames were captured every 10 s for 1 h, every 1 min for 1 h, every 2 min for 150 min, and every 30 min for 36 h. This was done to visualize the diffusive mixing of the inks in the simple microfluidic system.

## ■ ASSOCIATED CONTENT

### Supporting Information

The Supporting Information is available free of charge at https://pubs.acs.org/doi/10.1021/acsomega.1c00282.

Annotated photographs of printer modifications, print homogeneity characterization procedure, alignment characterization procedure, microcontainer chip-alignment method, microfluidic device design and experimental setup, and agar plate inserts for the inkjet printer (PDF)

## ■ AUTHOR INFORMATION


### Corresponding Author

**Nikolaj Kofoed Mandsberg** − *Center for Intelligent Drug Delivery and Sensing Using Microcontainers and Nanomechanics (IDUN), Department of Health Technology, Technical University of Denmark, 2800 Kgs Lyngby, Denmark*; orcid.org/0000-0003-3285-3887; Email: nikoma@dtu.dk

### Authors

**Jesper Højgaard** − *Center for Intelligent Drug Delivery and Sensing Using Microcontainers and Nanomechanics (IDUN), Department of Health Technology, Technical University of Denmark, 2800 Kgs Lyngby, Denmark*

**Shreya Suhas Joshi** − *Center for Intelligent Drug Delivery and Sensing Using Microcontainers and Nanomechanics (IDUN), Department of Health Technology, Technical University of Denmark, 2800 Kgs Lyngby, Denmark*

**Line Hagner Nielsen** − *Center for Intelligent Drug Delivery and Sensing Using Microcontainers and Nanomechanics (IDUN), Department of Health Technology, Technical University of Denmark, 2800 Kgs Lyngby, Denmark*; orcid.org/0000-0002-3789-4816

**Anja Boisen** − *Center for Intelligent Drug Delivery and Sensing Using Microcontainers and Nanomechanics (IDUN), Department of Health Technology, Technical University of Denmark, 2800 Kgs Lyngby, Denmark*

**En Te Hwu** − *Center for Intelligent Drug Delivery and Sensing Using Microcontainers and Nanomechanics (IDUN), Department of Health Technology, Technical University of Denmark, 2800 Kgs Lyngby, Denmark*

Complete contact information is available at:




https://dx.doi.org/10.1021/acsomega.1c00282
ACS Omega 2021, 6, 7786−7794

https://pubs.acs.org/10.1021/acsomega.1c00282

### Author Contributions

N.K.M. contributed in the conceptualization, methodology, software, formal analysis, investigation, writing of the original draft, visualization, and funding acquisition. J.H. contributed in the methodology and investigation. S.S.J. contributed in the investigation. L.H.N. contributed in writing (review & editing) and supervision. A.B. contributed in writing (review and editing), supervision, project administration, and funding acquisition. E.T.H. contributed in the conceptualization, investigation, resources, writing (review & editing), and supervision.

### Notes

The authors declare no competing financial interest.

## ■ ACKNOWLEDGMENTS

The authors would like to acknowledge the financial support from the Danish National Research Foundation (DNRF122), Villum Foundation (grant no. 9301) for Intelligent Drug Delivery and Sensing Using Microcontainers and Nanomechanics (IDUN), and the Novo Nordisk Foundation (NNF17OC0026910)—Microstructures, microbiota and oral delivery (MIMIO). N.K.M. is supported by an Excellence Ph.D. Scholarship from DTU Health Tech. The authors would also like to thank Lasse Højlund Eklund Thamdrup from the Department of Health Technology, Technical University of Denmark, for his help with the preparation of the microcontainers. Furthermore, the authors acknowledge the help from Lars Schulte for printer debugging; Daniel Andre Bunckenburg for assistance at the drug loading demonstration; and Anders Meyer Torp, Stine Egebro Hansen, and Priscila Guerra for input and help with the idea about screening for combinatorial minimum inhibition concentrations.

## ■ REFERENCES

(1) Park, J.; Moon, J.; Shin, H.; Wang, D.; Park, M. Direct-Write Fabrication of Colloidal Photonic Crystal Microarrays by Ink-Jet Printing. *J. Colloid Interface Sci.* **2006**, *298*, 713−719.

(2) Park, J.; Moon, J. Control of Colloidal Particle Deposit Patterns within Picoliter Droplets Ejected by Ink-Jet Printing. *Langmuir* **2006**, *22*, 3506−3513.

(3) Wang, L.; Wang, J.; Huang, Y.; Liu, M.; Kuang, M.; Li, Y.; Jiang, L.; Song, Y. Inkjet Printed Colloidal Photonic Crystal Microdot with Fast Response Induced by Hydrophobic Transition of Poly(N-Isopropyl Acrylamide). *J. Mater. Chem.* **2012**, *22*, 21405−21411.

(4) Cui, L.; Li, Y.; Wang, J.; Tian, E.; Zhang, X.; Zhang, Y.; Song, Y.; Jiang, L. Fabrication of Large-Area Patterned Photonic Crystals by Ink-Jet Printing. *J. Mater. Chem.* **2009**, *19*, 5499−5502.

(5) Xu, T.; Zhao, W.; Zhu, J. M.; Albanna, M. Z.; Yoo, J. J.; Atala, A. Complex Heterogeneous Tissue Constructs Containing Multiple Cell Types Prepared by Inkjet Printing Technology. *Biomaterials* **2013**, *34*, 130−139.

(6) Komuro, N.; Takaki, S.; Suzuki, K.; Citterio, D. Inkjet Printed (Bio)Chemical Sensing Devices. *Anal. Bioanal. Chem.* **2013**, *405*, 5785−5805.

(7) Fox, C. B.; Nemeth, C. L.; Chevalier, R. W.; Cantlon, J.; Bogdanoff, D. B.; Hsiao, J. C.; Desai, T. A. Picoliter-Volume Inkjet Printing into Planar Microdevice Reservoirs for Low-Waste, High-Capacity Drug Loading. *Bioeng. Transl. Med.* **2017**, *2*, 9−16.

(8) Nemeth, C. L.; Lykins, W. R.; Tran, H.; ElSayed, M. E. H.; Desai, T. A. Bottom-Up Fabrication of Multilayer Enteric Devices for the Oral Delivery of Peptides. *Pharm. Res.* **2019**, *36*, 89.

(9) Chirra, H. D.; Shao, L.; Ciaccio, N.; Fox, C. B.; Wade, J. M.; Ma, A.; Desai, T. A. Planar Microdevices for Enhanced In Vivo Retention and Oral Bioavailability of Poorly Permeable Drugs. *Adv. Healthcare Mater.* **2014**, *3*, 1648−1654.

(10) Marizza, P.; Keller, S. S.; Boisen, A. Inkjet Printing as a Technique for Filling of Micro-Wells with Biocompatible Polymers. *Microelectron. Eng.* **2013**, *111*, 391−395.

(11) Marizza, P.; Keller, S. S.; Müllertz, A.; Boisen, A. Polymer-Filled Microcontainers for Oral Delivery Loaded Using Supercritical Impregnation. *J. Controlled Release* **2014**, *173*, 1−9.

(12) Zhu, X.; Zheng, Q.; Yang, H.; Cai, J.; Huang, L.; Duan, Y.; Xu, Z.; Cen, P. Recent Advances in Inkjet Dispensing Technologies: Applications in Drug Discovery. *Expert Opin. Drug Discov.* **2012**, *7*, 761−770.

(13) Chitnis, G.; Ding, Z.; Chang, C. L.; Savran, C. A.; Ziaie, B. Laser-Treated Hydrophobic Paper: An Inexpensive Microfluidic Platform. *Lab on a Chip* **2011**, *11*, 1161−1165.

(14) Sun, Y.; Chen, X.; Zhou, X.; Zhu, J.; Yu, Y. Droplet-in-Oil Array for Picoliter-Scale Analysis Based on Sequential Inkjet Printing. *Lab Chip* **2015**, *15*, 2429−2436.

(15) Sun, Y.; Zhou, X.; Yu, Y. A Novel Picoliter Droplet Array for Parallel Real-Time Polymerase Chain Reaction Based on Double-Inkjet Printing. *Lab Chip* **2014**, *14*, 3603−3610.

(16) Guo, Y.; Li, L.; Li, F.; Zhou, H.; Song, Y. Inkjet Print Microchannels Based on a Liquid Template. *Lab Chip* **2015**, *15*, 1759−1764.

(17) Elsharkawy, M.; Schutzius, T. M.; Megaridis, C. M. Inkjet Patterned Superhydrophobic Paper for Open-Air Surface Microfluidic Devices. *Lab Chip* **2014**, *14*, 1168−1175.

(18) Su, W.; Cook, B. S.; Fang, Y.; Tentzeris, M. M. Fully Inkjet-Printed Microfluidics: A Solution to Low-Cost Rapid Three-Dimensional Microfluidics Fabrication with Numerous Electrical and Sensing Applications. *Sci. Rep.* **2016**, *6*, 35111.

(19) Yoo, M.; Kim, H. K.; Kim, S.; Tentzeris, M.; Lim, S. Silver Nanoparticle-Based Inkjet-Printed Metamaterial Absorber on Flexible Paper. *IEEE Antennas Wirel. Propag. Lett.* **2015**, *14*, 1718−1721.

(20) Farooqui, M. F.; Shamim, A. Low Cost Inkjet Printed Smart Bandage for Wireless Monitoring of Chronic Wounds. *Sci. Rep.* **2016**, *6*, 28949.

(21) Khan, A.; Roo, J. S.; Kraus, T.; Steimle, J. *Proceedings of the 32nd Annual {ACM} Symposium on User Interface Software and Technology*; Guimbretière, F., Bernstein, M., Reinecke, K., Eds.; UIST: New Orleans, LA, USA, 2019, October 20−23, 2019; *ACM*, 2019; pp. 341−354. DOI: 10.1145/3332165.

(22) Sartori, A. F.; Belardinelli, P.; Dolleman, R. J.; Steeneken, P. G.; Ghatkesar, M. K.; Buijnsters, J. G. Inkjet-Printed High-Q Nanocrystalline Diamond Resonators. *Small* **2019**, *15*, 1803774.

(23) Cho, H.; Parameswaran, M. A.; Yu, H.-Z. Fabrication of Microsensors Using Unmodified Office Inkjet Printers. *Sens. Actuators, B* **2007**, *123*, 749−756.

(24) Creran, B.; Li, X.; Duncan, B.; Kim, C. S.; Moyano, D. F.; Rotello, V. M. Detection of Bacteria Using Inkjet-Printed Enzymatic Test Strips. *ACS Appl. Mater. Interfaces* **2014**, *6*, 19525−19530.

(25) Balu, B.; Berry, A. D.; Hess, D. W.; Breedveld, V. Patterning of Superhydrophobic Paper to Control the Mobility of Micro-Liter Drops for Two-Dimensional Lab-on-Paper Applications. *Lab Chip* **2009**, *9*, 3066−3075.

(26) Barona, D.; Amirfazli, A. Producing a Superhydrophobic Paper and Altering Its Repellency through Ink-Jet Printing. *Lab Chip* **2011**, *11*, 936−940.

(27) Watanabe, M. Microfluidic Devices Easily Created Using an Office Inkjet Printer. *Microfluid. Nanofluid.* **2010**, *8*, 403−408.

(28) Dixon, C.; Ng, A. H. C.; Fobel, R.; Miltenburg, M. B.; Wheeler, A. R. An Inkjet Printed, Roll-Coated Digital Microfluidic Device for Inexpensive, Miniaturized Diagnostic Assays. *Lab Chip* **2016**, *16*, 4560−4568.

(29) Li, X.; Shi, M.; Cui, C.; Yu, H. Z. Inkjet-Printed Bioassays for Direct Reading with a Multimode DVD/Blu-Ray Optical Drive. *Anal. Chem.* **2014**, *86*, 8922−8926.

(30) Cohen, D. J.; Morfino, R. C.; Maharbiz, M. M. A Modified Consumer Inkjet for Spatiotemporal Control of Gene Expression. *PLoS One* **2009**, *4*, e7086.
(31) Kumar, S.; Bhat, V.; Vinoy, K. J.; Santhanam, V. Using an Office Inkjet Printer to Define the Formation of Copper Films on Paper. *IEEE Trans. Nanotechnol.* **2014**, *13*, 160−164.
(32) Dixon, C.; Lamanna, J.; Wheeler, A. R. Direct Loading of Blood for Plasma Separation and Diagnostic Assays on a Digital Microfluidic Device. *Lab Chip* **2020**, *20*, 1845−1855.
(33) Li, H.; Huang, Y.; Wei, Z.; Wang, W.; Yang, Z.; Liang, Z.; Li, Z. An Oligonucleotide Synthesizer Based on a Microreactor Chip and an Inkjet Printer. *Sci. Rep.* **2019**, *9*, 5058.
(34) Yakovlev, A. V.; Milichko, V. A.; Pidko, E. A.; Vinogradov, V. V.; Vinogradov, A. V. Inkjet Printing of TiO2/AlOOH Heterostructures for the Formation of Interference Color Images with High Optical Visibility. *Sci. Rep.* **2016**, *6*, 37090.
(35) You, M.; Zhong, J.; Hong, Y.; Duan, Z.; Lin, M.; Xu, F. Inkjet Printing of Upconversion Nanoparticles for Anti-Counterfeit Applications. *Nanoscale* **2015**, *7*, 4423−4431.
(36) Waasdorp, R.; Van Den Heuvel, O.; Versluis, F.; Hajee, B.; Ghatkesar, M. K. Accessing Individual 75-Micron Diameter Nozzles of a Desktop Inkjet Printer to Dispense Picoliter Droplets on Demand. *RSC Adv.* **2018**, *8*, 14765−14774.
(37) Mandsberg, N. K.; Hansen, O.; Taboryski, R. Generation of Micro-Droplet Arrays by Dip-Coating of Biphilic Surfaces ; the Dependence of Entrained Droplet Volume on Withdrawal Velocity. *Sci. Rep.* **2017**, *7*, 12794.
(38) Ueda, E.; Geyer, F. L.; Nedashkivska, V.; Levkin, P. A. DropletMicroarray: Facile Formation of Arrays of Microdroplets and Hydrogel Micropads for Cell Screening Applications. *Lab Chip* **2012**, *12*, 5218−5224.
(39) Mandsberg, N. K.; Taboryski, R. Spatial Control of Condensation on Chemically Homogeneous Pillar-Built Surfaces. *Langmuir* **2017**, *33*, 5197−5203.
(40) Martinez, A. W.; Phillips, S. T.; Butte, M. J.; Whitesides, G. M. Patterned Paper as a Platform for Inexpensive, Low-Volume, Portable Bioassays**. *Angew. Chem., Int. Ed.* **2007**, *46*, 1318−1320.
(41) Martinez, A. W.; Phillips, S. T.; Nie, Z.; Cheng, C. M.; Carrilho, E.; Wiley, B. J.; Whitesides, G. M. Programmable Diagnostic Devices Made from Paper and Tape. *Lab Chip* **2010**, *10*, 2499−2504.
(42) Nie, Z.; Nijhuis, C. A.; Gong, J.; Chen, X.; Kumachev, A.; Martinez, A. W.; Narovlyansky, M.; Whitesides, G. M. Electrochemical Sensing in Paper-Based Microfluidic Devices. *Lab Chip* **2010**, *10*, 477−483.
(43) Unno, N.; Satake, S. I.; Taniguchi, J. Super-Resolution Technique for Nanoimprint Mold Using Elastic UV-Curable Resin. *Microelectron. Eng.* **2013**, *110*, 167−172.
(44) Yokoo, A.; Wada, K.; Kimerling, L. C. Pattern Size Reduction of Nanoprint-Fabricated Structures on Heat-Shrinkable Film. *Jpn. J. Appl. Phys.* **2007**, *46*, 6395−6397.
(45) Hatton, B.; Mishchenko, L.; Davis, S.; Sandhage, K. H.; Aizenberg, J. Assembly of Large-Area, Highly Ordered, Crack-Free Inverse Opal Films. *Proc. Natl. Acad. Sci. U. S. A.* **2010**, *107*, 10354−10359.
(46) Walsh, E. J.; Feuerborn, A.; Wheeler, J. H. R.; Tan, A. N.; Durham, W. M.; Foster, K. R.; Cook, P. R. Microfluidics with Fluid Walls. *Nat. Commun.* **2017**, 816.
(47) Nielsen, L. H.; Keller, S. S.; Boisen, A. Microfabricated Devices for Oral Drug Delivery. *Lab Chip* **2018**, 2348−2358.
(48) Mandsberg, N. K.; Christfort, J. F.; Kamguyan, K.; Boisen, A.; Srivastava, S. K. Orally Ingestible Medical Devices for Gut Engineering. *Adv. Drug Delivery Rev.* **2020**, 142.
(49) Ainslie, K. M.; Lowe, R. D.; Beaudette, T. T.; Petty, L.; Bachelder, E. M.; Desai, T. A. Microfabricated Devices for Enhanced Bioadhesive Drug Delivery: Attachment to and Small-Molecule Release through a Cell Monolayer under Flow. *Small* **2009**, *5*, 2857−2863.
(50) Sant, S.; Tao, S. L.; Fisher, O. Z.; Xu, Q.; Peppas, N. A.; Khademhosseini, A. Microfabrication Technologies for Oral Drug Delivery. *Adv. Drug Delivery Rev.* **2012**, *64*, 496−507.
(51) Ainslie, K. M.; Kraning, C. M.; Desai, T. A. Microfabrication of an Asymmetric, Multi-Layered Microdevice for Controlled Release of Orally Delivered Therapeutics. *Lab Chip* **2008**, 1042.
(52) Biswas, T. T.; Yu, J.; Nierstrasz, V. A. Effects of Ink Characteristics and Piezo-Electric Inkjetting Parameters on Lysozyme Activity. *Sci. Rep.* **2019**, *9*, 18252.
(53) Thomas, C. R.; Geer, D. Effects of Shear on Proteins in Solution. *Biotechnol. Lett.* **2011**, *33*, 443−456.
(54) Huh, K. M.; Kang, H. C.; Lee, Y. J.; Bae, Y. H. PH-Sensitive Polymers for Drug Delivery. *Macromol. Res.* **2012**, *20*, 224−233.
(55) Kosaraju, S. L. Colon Targeted Delivery Systems: Review of Polysaccharides for Encapsulation and Delivery. *Crit. Rev. Food Sci. Nutr.* **2005**, *45*, 251−258.
(56) Göpferich, A. Mechanisms of Polymer Degradation and Erosion. *Biomaterials* **1996**, *17*, 103−114.
(57) Foresti, D.; Kroll, K. T.; Amissah, R.; Sillani, F.; Homan, K. A.; Poulikakos, D.; Lewis, J. A. Acoustophoretic Printing. *Sci. Adv.* **2018**, *4*, eaat1659.
(58) Heo, Y. S.; Lee, H. J.; Hassell, B. A.; Irimia, D.; Toth, T. L.; Elmoazzen, H.; Toner, M. Controlled Loading of Cryoprotectants (CPAs) to Oocyte with Linear and Complex CPA Profiles on a Microfluidic Platform. *Lab Chip* **2011**, *11*, 3530−3537.
(59) Xu, T.; Jin, J.; Gregory, C.; Hickman, J. J.; Boland, T. Inkjet Printing of Viable Mammalian Cells. *Biomaterials* **2005**, *26*, 93−99.
(60) Yoon, S.-H.; Lee, S.-G.; Cho, M.-O.; Kim, J.-K. Two-Dimensional Patterning of Bacteria by Inkjet Printer. *Trans. Kor. Soc. Mech. Eng. B* **2010**, *34*, 89−94.
(61) Jeon, S.; Park, S.; Nam, J.; Kang, Y.; Kim, J. M. Creating Patterned Conjugated Polymer Images Using Water-Compatible Reactive Inkjet Printing. *ACS Appl. Mater. Interfaces* **2016**, *8*, 1813−1818.
(62) Van Osch, T. H. J.; Perelaer, J.; De Laat, A. W. M.; Schubert, U. S. Inkjet Printing of Narrow Conductive Tracks on Untreated Polymeric Substrates. *Adv. Mater.* **2008**, *20*, 343−345.
(63) Bai, L.; Mai, V. C.; Lim, Y.; Hou, S.; Möhwald, H.; Duan, H. Large-Scale Noniridescent Structural Color Printing Enabled by Infiltration-Driven Nonequilibrium Colloidal Assembly. *Adv. Mater.* **2018**, *30*, 1705667.
(64) Modak, C. D.; Kumar, A.; Tripathy, A.; Sen, P. Drop Impact Printing. *Nat. Commun.* **2020**, *11*, 4327.
(65) Yu, Y.; Brandt, S.; Nicolas, N. J.; Aizenberg, J. Colorimetric Ethanol Indicator Based on Instantaneous, Localized Wetting of a Photonic Crystal. *ACS Appl. Mater. interfaces* **2019**, 1924.
(66) Han, X.; Wang, L.; Wang, X. Fabrication of Chemical Gradient Using Space Limited Plasma Oxidation and Its Application for Droplet Motion. *Adv. Funct. Mater.* **2012**, *22*, 4533−4538.
(67) Lei, W.; Demir, K.; Overhage, J.; Grunze, M.; Schwartz, T.; Levkin, P. A. Droplet-Microarray: Miniaturized Platform for High-Throughput Screening of Antimicrobial Compounds. *Adv. Biosys.* **2020**, *4*, 2000073.
(68) Aizenberg, J.; Black, A. J.; Whitesides, G. M. Control of Crystal Nucleation by Patterned Self-Assembled Monolayers. *Nature* **1999**, *398*, 495−498.
(69) Okeyo, P. O.; Larsen, P. E.; Kissi, E. O.; Ajalloueian, F.; Rades, T.; Rantanen, J.; Boisen, A. Single Particles as Resonators for Thermomechanical Analysis. *Nat. Commun.* **2020**, *11*, 1235.
(70) Nielsen, L. H.; Keller, S. S.; Gordon, K. C.; Boisen, A.; Rades, T.; Müllertz, A. Spatial Confinement Can Lead to Increased Stability of Amorphous Indomethacin. *Eur. J. Pharm. Biopharm.* **2012**, *81*, 418−425.
(71) EPSON. *EPSON ink product information sheet*. https://files.support.epson.com/pdf/msds/t664120.pdf (accessed Sep 29, 2020).


https://dx.doi.org/10.1021/acsomega.1c00282
*ACS Omega* 2021, 6, 7786−7794